ISSN 1674-1056
http://cpb.iphy.ac.cn
http://iopscience.iop.org/cpb
中国物理 B
Chinese Physics
中国物理
Chinese Physics B

Strong anti-strain capacity of CoFeB/MgO interface on electronic structure and state coupling

Fei Guo(郭飞), Yaping Wu(吴雅苹), Zhiming Wu(吴志明), Ting Chen(陈婷), Heng Li(李恒), Chunmiao Zhang(张纯淼), Mingming Fu(付明明), Yihong Lu(卢奕宏), Junyong Kang(康俊勇)
Citation: Chin. Phys. B . 2018, 27(1): 017502. **doi:** 10.1088/1674-1056/27/1/017502

Journal homepage: http://cpb.iphy.ac.cn; http://iopscience.iop.org/cpb

What follows is a list of articles you may be interested in

Role of vacancy-type defects in magnetism of GaMnN

Hai-Ying Xing(邢海英), Yu Chen(陈雨), Chen Ji(纪骋), Sheng-Xiang Jiang(蒋盛翔), Meng-Yao Yuan(苑梦尧), Zhi-Ying Guo(郭志英), Kun Li(李琨), Ming-Qi Cui(崔明启), Guo-Yi Zhang(张国义)
Chin. Phys. B . 2016, 25(6): 067503. **doi:** 10.1088/1674-1056/25/6/067503

Effect of exchange coupling on magnetic property in Sm-Co/*α*-Fe layered system

C X Sang(桑成祥), G P Zhao(赵国平), W X Xia(夏卫星), X L Wan(万秀琳), F J Morvan, X C Zhang(张溪超), L H Xie(谢林华), J Zhang(张健), J Du(杜娟), A R Yan(闫阿儒), P Liu(刘平)
Chin. Phys. B . 2016, 25(3): 037501. **doi:** 10.1088/1674-1056/25/3/037501

Magnetic–optical bifunctional $CoPt_3$/Co multilayered nanowire arrays

Su Yi-Kun, Yan Zhi-Long, Wu Xi-Ming, Liu Huan, Ren Xiao, Yang Hai-Tao
Chin. Phys. B . 2015, 24(10): 107505. **doi:** 10.1088/1674-1056/24/10/107505

Tailoring the structural and magnetic properties of Cu-doped ZnO by *c*-axis pressure

Gong Ji-Jun, Chen Ji-Pei, Zhang Fei, Wu Hao, Qin Ming-Hui, Zeng Min, Gao Xing-Sen, Liu Jun-Ming
Chin. Phys. B . 2015, 24(3): 037505. **doi:** 10.1088/1674-1056/24/3/037505

Electron-mediated ferromagnetism in Fe-doped InP: Theory and experiment

Dong Shan, Zhu Feng
Chin. Phys. B . 2012, 21(9): 097502. **doi:** 10.1088/1674-1056/21/9/097502

Strong anti-strain capacity of CoFeB/MgO interface on electronic structure and state coupling*

Fei Guo(郭飞), Yaping Wu(吴雅苹)†, Zhiming Wu(吴志明)‡, Ting Chen(陈婷), Heng Li(李恒), Chunmiao Zhang(张纯淼), Mingming Fu(付明明), Yihong Lu(卢奕宏), and Junyong Kang(康俊勇)¶

Collaborative Innovation Center for Optoelectronic Semiconductors and Efficient Devices, Fujian Provincial Key Laboratory of Semiconductors and Applications, Department of Physics, Xiamen University, Xiamen 361005, China

(Received 8 May 2017; revised manuscript received 9 August 2017; published online 17 November 2017)

Electronic structure and spin-related state coupling at ferromagnetic material (FM)/MgO (FM = Fe, CoFe, CoFeB) interfaces under biaxial strain are evaluated using the first-principles calculations. The CoFeB/MgO interface, which is superior to the Fe/MgO and CoFe/MgO interfaces, can markedly maintain stable and effective coupling channels for majority-spin Δ_1 state under large biaxial strain. Bonding interactions between Fe, Co, and B atoms and the electron transfer between Bloch states are responsible for the redistribution of the majority-spin Δ_1 state, directly influencing the coupling effect for the strained interfaces. Layer-projected wave function of the majority-spin Δ_1 state suggests slower decay rate and more stable transport property in the CoFeB/MgO interface, which is expected to maintain a higher tunneling magnetoresistance (TMR) value under large biaxial strain. This work reveals the internal mechanism for the state coupling at strained FM/MgO interfaces. This study may provide some references to the design and manufacturing of magnetic tunnel junctions with high tunneling magnetoresistance effect.

Keywords: ferromagnet material/MgO interface, biaxial strain, state coupling, first-principles calculation

PACS: 75.70.Cn, 72.25.Mk, 72.25.–b, 73.20.–r **DOI:** 10.1088/1674-1056/27/1/017502

1. Introduction

Tunneling magnetoresistance (TMR) effect in magnetic tunnel junctions (MTJs) has been intensively studied because of the wide application of MTJs in spintronics,[1–5] such as magnetic random access memory,[6] high-frequency microwave sources,[7] and magnetic sensors.[8,9] Theoretically, the TMR ratio is directly related to the spin polarization of the tunneling electrons in ferromagnetic material (FM) electrodes[10] and the tunneling matrix elements of the spin electrons.[11] Four-fold symmetry at the electrode/barrier interface is essential for common MgO-based MTJs[12] to realize a large TMR effect.[13–15] Different magnetic materials have been employed as the FM electrodes. For example, Yuasa *et al.* fabricated Fe/MgO/Fe MTJs using molecular beam epitaxy and obtained TMR ratios of 180% and 247% at 293 K and 20 K, respectively. However, numerous dislocations formed at the interface because of the large lattice mismatch between Fe and MgO,[16] resulting in low performance. Parking *et al.* adopted CoFe alloy as the FM layers to improve the crystallinity and achieved TMR ratio up to 220% at room temperature and 300% at 4 K.[17,18] Currently, the CoFeB material is the most frequently used material in the FM electrode, and the recorded TMR ratios of CoFeB are 604% at 300 K and 1144% at 5 K.[19] However, the experimental value remains far below the predicted one exceeding 10000%,[13,14] and most studies show that interfacial oxidations,[20] oxygen vacancies in the MgO barrier,[21,22] and interfacial dislocations are responsible for the low TMR ratio. Thus, several attempts, such as insertion of Mg atoms or introduction of B atoms at the interface, were performed, which improved the TMR effect to a certain extent.[23–25] In addition, several studies have shown that the epitaxial strain can also affect the magnetocrystalline anisotropy [26,27] and TMR effect.[28] Bonell *et al.* reported the enhanced TMR effect in $Fe_{0.9}V_{0.1}$/MgO/Fe MTJ by replacing the Fe electrode with the Fe–V alloy, which led to a smaller mismatch.[29] Löhndorf *et al.* developed a highly sensitive strain sensor based on the strain effect in MgO MTJ, in which a 0.04% change in strain results in a change of 24% in resistance.[20] However, the strain effect on the FM/MgO interfacial state coupling, which affects the TMR ratio of MgO-based MTJs, remains unclear. Investigating the spin-dependence state coupling of the FM/MgO interfaces and understanding the internal mechanism under intrinsic strain are of particular significance for designing the FM/MgO in-

*Project supported by the National Key Research and Development Program of China (Grant No. 2016YFB0400801), the National Natural Science Foundation of China (Grant Nos. 61774128, 61674124, 11604275, 11304257, and 61227009), the Natural Science Foundation of Fujian Province of China (Grant Nos. 2017J01012, 2014J01026, 2016J01037, and 2015J01028), and the Fundamental Research Funds for the Central Universities, China (Grant Nos. 20720150027, 20720160044, 20720160122, 20720170085,20720170012, and 20720150033).

†Corresponding author. E-mail: ypwu@xmu.edu.cn

‡Corresponding author. E-mail: zmwu@xmu.edu.cn

¶Corresponding author. E-mail: jykang@xmu.edu.cn

© 2018 Chinese Physical Society and IOP Publishing Ltd

terface and further improving the TMR ratio of MgO-based MTJs.

In this work, we study the effects of the intrinsic interfacial strain on the state coupling in FM/MgO (FM = Fe, CoFe, CoFeB) interfaces by using the first-principles calculations. The $k_{||}$-resolved density of the majority-spin Δ_1 state is calculated to study the strain-dependent coupling effect between the FM and MgO layers. The decomposed electronic local densities of states (DOS) and the orbital polarization are used to clarify the interfacial interaction and electron transfer under the strain. The layer-projected wave function of the majority-spin Δ_1 Bloch state is further calculated to estimate the relative TMR value of the MTJ. Considering that the biaxial strain commonly exists because of lattice mismatch, this work reveals the state coupling performance of the FM/MgO interface. Moreover, the internal mechanism is explained from the perspective of the biaxial strain. Thus, this study may provide some references to the design and manufacturing of MgO-based MTJs with enhanced TMR effect.

2. Computational details

We perform the density functional theory (DFT)[30–32] calculations with the Vienna *ab initio* simulation package code,[33] using the projector-augmented wave pseudopotential method.[34,35] Slab models are constructed for all FM/MgO interfacial calculations. These models contain eight FM atom layers, three MgO layers, and a vacuum distance of 15 Å. The exchange and correlation effects are treated by Perdew–Burke–Ernzerhof (PBE) generalized gradient approximation.[36] The plane-wave cutoff energy is set to 520 eV, which provides a good total energy convergence of approximately 1 meV/atom. The Brillouin zone is sampled according to the Monkhorst–Pack method.[37] The Fermi discontinuity is smoothed using the Methfessel–Paxton smearing[38] with a broadening parameter of 0.01 eV to improve the k-points convergence. The number of k-points is selected to provide a total energy convergence similar to that of the cutoff energy. Structural relaxations are performed to ensure that the Hellmann–Feynman forces acting on the ions are less than 0.001 eV/Å. The Hubbard U is estimated to generate a tiny effect on the results, and thus is omitted in the present work. The two bottom layers are fixed at the theoretical bulk position to represent the semi-infinite bulk beneath the interface, and the other atomic layers are fully relaxed. The Fe/MgO interface involves two different configurations, namely, the Fe atom sits on top of O or Mg atom.[39–41] Based on the total energy calculations, the configuration shown in Fig. 1(a) is energetically preferred. For the $Co_{0.25}Fe_{0.75}$/MgO (hereafter simply named as CoFe/MgO) interface, the CoFe electrode with 25% Co and 75% Fe is an optimized composition producing the highest TMR ratio.[19] The CoFe/MgO interface also involves two highly symmetrical configurations, in which the Co atom may locate at the interfacial layer or not. According to the total energy, the configuration with both Co and Fe atoms in the interfacial layer is more stable (Fig. 1(b)). For the CoFeB/MgO interface, the small B atom may occupy the center of the tetrahedral or octahedral interstitial site of the CoFe electron, where the latter is energetically favorable (Fig. 1(c)).

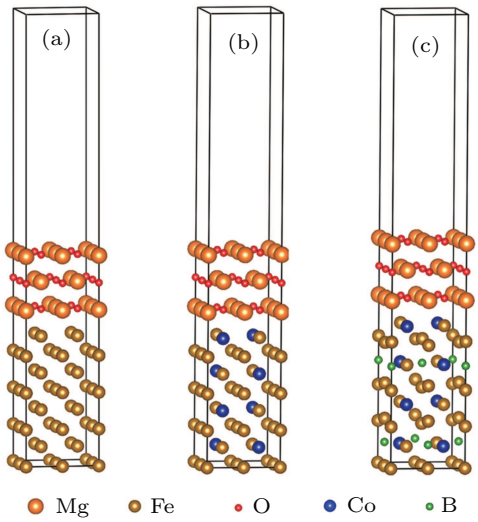


Fig. 1. (color online) Stable configurations of Fe/MgO, CoFe/MgO, and CoFeB/MgO interfaces. (a) O atoms sit atop the Fe atom for the Fe/MgO interface, (b) the Co and Fe atoms appear in the interfacial layer for the CoFe/MgO interface, and (c) B atom locates in the octahedral interstitial site for the CoFeB/MgO interface. The orange, brownish yellow, red, blue, and green balls represent Mg, Fe, O, Co, and B atoms, respectively.

3. Results and discussion

A biaxial tensile strain is applied and gradually increased to 3.5% based on the stable configurations of the three FM/MgO interfaces. The applied strain is defined as $\varepsilon = (a - a_0)/a_0$, where a and a_0 are the xy-plane lattice constants for the strained and unstrained structures, respectively. The lattice constants of the FM metals are used as the a_0 values for the FM/MgO interfaces. The lattice constants from the DFT-PBE calculations for the bulk FM metals are 2.831 Å and 2.849 Å for bcc-Fe and CoFe, respectively. These results are consistent with the previous studies.[42,43] Considering that the small B atom occupies the center of the octahedral interstitial site of the CoFe electron, the lattice constant of bulk CoFe is approximately adopted for the CoFeB/MgO unstrained lattice constants.

Generally, an expansion applied in a direction results in the compression in the transverse direction, the biaxial strains in the xy-plane, and the transverse response in the z-direction. The optimized FM–O bonds in the three FM/MgO interfaces under the biaxial strain are shown in Table 1. The stability

of atomic structure of the three FM/MgO interfaces under the biaxial strain is evaluated. The Fe–O equilibrium distance for the unstrained Fe/MgO interface is 2.191 Å, consistent with the previous results.[44,45] The interfacial O atom of the unstrained CoFe/MgO interface bonds to both Fe and Co atoms with bond lengths of 2.103 Å and 2.224 Å, respectively. The shorter bond length of Fe–O in the CoFe/MgO interface suggests stronger interaction between O and Fe atoms than that in the Fe/MgO interface. The bond lengths of Fe–O and Co–O in the unstrained CoFeB/MgO interface are 2.126 Å and 2.227 Å, respectively, larger than the values in the CoFe/MgO interface. This result indicates that introducing B atoms slightly weakens the interaction between the interfacial Fe(Co) and O atoms. All FM–O bond lengths decrease when the biaxial tension strain is applied to the three FM/MgO interfaces. Among the three interfaces, the bond lengths of Fe(Co)–O in the CoFeB/MgO exhibit the minimum change when the biaxial strain is increased. This result suggests that the CoFeB/MgO interface has higher geometry structural stability, which is conducive to retain the stability of the electronic properties compared with the other two interfaces.

Table 1. Optimized FM–O bond lengths (Å) in the three FM/MgO (FM = Fe, CoFe, and CoFeB) interfaces under different biaxial strains.

Biaxial strain	Fe/MgO	CoFe/MgO		CoFeB/MgO	
	Fe–O	Fe–O	Co–O	Fe–O	Co–O
0%	2.191	2.103	2.224	2.126	2.227
1.4%	2.169	2.084	2.195	2.119	2.196
2.8%	2.143	2.066	2.170	2.106	2.183
3.5%	2.126	2.050	2.144	2.098	2.178

For the MgO based MTJ, the dominant contribution of tunneling conductance is from the Δ_1 state of the majority spin channel. The full spin-polarization of the Δ_1 state is of crucial importance for the spin-polarized transport properties.[14,46] Given this, partial DOS (that corresponds to the Δ_1 state in the majority spin channel) near the FM–MgO interface under various biaxial strains is calculated to infer the strain-dependent coupling efficiency between the FM and MgO layers. Figures 2 and 3 illustrate the $k_{||}$-resolved partial DOS of the majority-spin Δ_1 state near the Fermi energy for interfacial Fe (Co) atoms in the three FM/MgO interfaces. According to Ref. [47], states with the same Bloch states at the two-dimensional Brillouin zone (2DBZ) have different decay rates for different $k_{||}$ values. For example, states far from the center of the 2DBZ decay faster than those close to the center. A strong peak of the majority-spin Δ_1 state for the interfacial Fe atom of the unstrained Fe/MgO interface locates at the center ($k_{||} = 0$) of the 2DBZ and is surrounded by four weaker peaks (Fig. 2(a)). The Δ_1 state of the Fe atom at the Fe/MgO interface is found to be sensitive to the biaxial strain. The centered and four surrounded peaks rapidly weaken and finally disappear as the biaxial strain gradually increases from 1.4% to 3.5% (Figs. 2(b)–2(d)). Therefore, the coupling efficiency of the majority-spin Δ_1 state between Fe and MgO layers decreases sharply as the biaxial strain increases, and the coupling channel will mostly be closed when the biaxial strain exceeds a threshold value of 2.8%. This result suggests that the interfacial biaxial strain induced by lattice mismatch plays an important role in the spin-dependent transport which should not be ignored in the Fe/MgO interface. The majority-spin Δ_1 state at the Fermi energy (Fig. 2(e)) in the interfacial Fe atom in the untrained CoFe/MgO interface is slightly weaker than that in the untrained Fe/MgO interface. However, as the biaxial strain increases, the decay rate of the centered peak at $k_{||} = 0$ obviously becomes slower (Figs. 2(e)–2(h)). Consequently, some majority-spin Δ_1 states remain located at the center of the 2DBZ under a biaxial strain of 3.5%. This essential difference from that of the Fe atom in the Fe/MgO interface implies that even under a large biaxial strain, the majority-spin Δ_1 state can also couple into the MgO barrier layer through the interfacial Fe atom for the CoFe/MgO interface. In addition to the Fe atoms, the interfacial Co atom also opens up a coupling channel between the CoFe electrode and MgO barrier layer. The centered peak of the majority-spin Δ_1 state decreases with increasing strain until the state finally disappears under 3.5% biaxial strain. The threshold value here is higher than that (2.8%) of the Fe atom in the Fe/MgO interface. Given the large biaxial strain induced by lattice mismatch, the majority-spin Δ_1 state can be more effectively coupled into MgO through CoFe electrode than through Fe electrode.

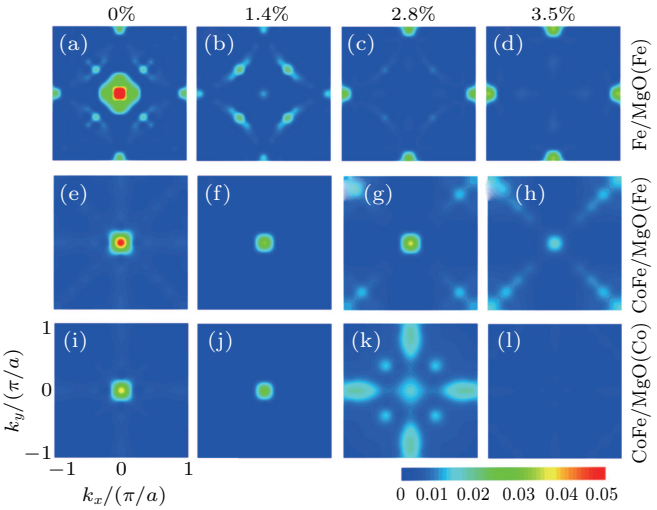


Fig. 2. (color online) $k_{||}$-resolved densities of state (DOS) at the interfacial Fe and Co atoms in the Fe/MgO and CoFe/MgO interfaces near the Fermi energy with Δ_1 symmetry. Majority-spin channels for the interfacial ((a)–(d)) Fe atom in the Fe/MgO interface, ((e)–(h)) Fe atom in the CoFe/MgO interface, and ((i)–(l)) Co atom in the CoFe/MgO interface. Left to right panels correspond to the biaxial strains of 0%, 1.4%, 2.8%, and 3.5%, respectively.

Although the CoFe is superior to the Fe electrode when

the large mismatch-strain is considered, the distinct decay of the majority-spin Δ_1 state still restricts the coupling efficiency between the electrode and barrier layer. Compared with these two interfaces, the CoFeB/MgO interface can markedly maintain the majority-spin Δ_1 state at the Fermi energy by introducing B atoms into the CoFe alloy electrode and thus keep a high coupling efficiency. The decay of the majority-spin Δ_1 state is obviously slower than that in the above two cases when the biaxial strain increases (Fig. 3). Even under a 3.5% biaxial strain, large coupling channels exist, with which the majority-spin Δ_1 state can effectively couple into MgO through both the interfacial Fe and Co atoms in the CoFeB/MgO interface.

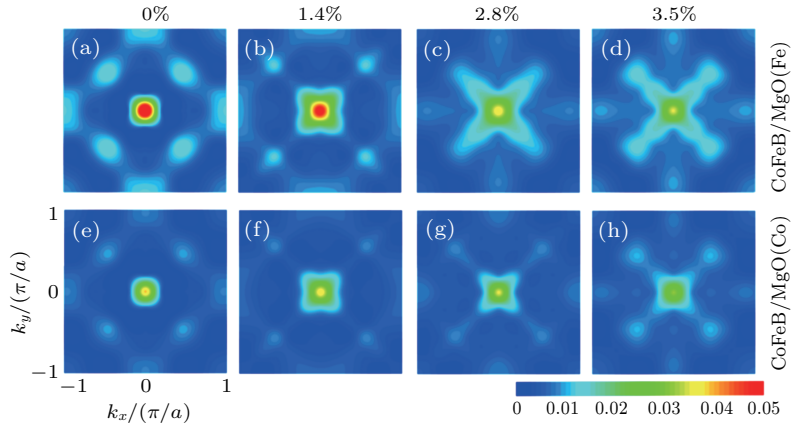


Fig. 3. (color online) $k_{||}$-resolved DOS at the interfacial Fe and Co atoms in the CoFeB/MgO interface near the Fermi energy with Δ_1 symmetry. Majority-spin channels for the interfacial ((a)–(d)) Fe and ((e)–(h)) Co atoms. Left to right panels correspond to the biaxial strains of 0%, 1.4%, 2.8%, and 3.5%, respectively.

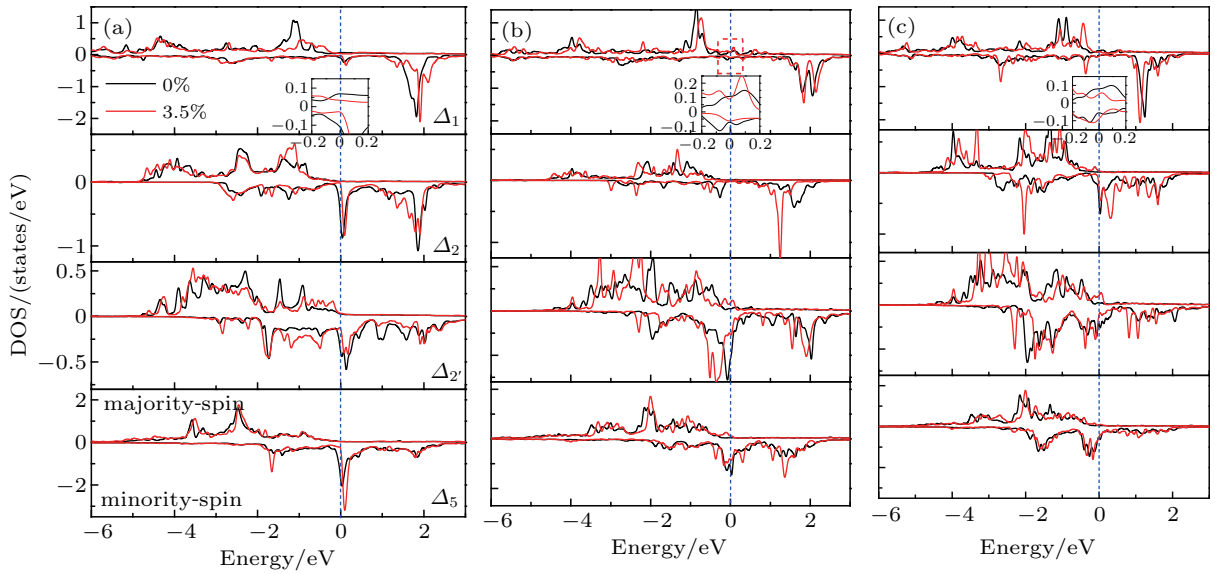


Fig. 4. (color online) Orbital-decomposed DOS for the interfacial (a) Fe atom in the Fe/MgO interface, (b) Fe atom in the CoFe/MgO interface, and (c) Co atom in the Fe/MgO interface. Details around E_F for the Δ_1 state are shown in the inset. The red and black lines correspond to the biaxial strains of 0% and 3.5%, respectively.

The origin of the redistribution of the majority-spin Δ_1 state under biaxial strain is further investigated by calculating the four spin-polarized Bloch states with different symmetries for the interfacial Fe (Co) atoms. Orbital-decomposed DOS of the interfacial Fe atom in the unstrained and 3.5% biaxial-strained Fe/MgO interfaces are shown in Fig. 4(a). The majority-spin Bloch states for all four symmetries are highly occupied, while the minority-spin states are partially occupied in both unstrained and strained Fe/MgO interfaces. Significant minority-spin states are located at the Fermi level for the Δ_2, $\Delta_{2'}$, and Δ_5 symmetries. This characteristic indicates that the minority-spin states are sensitive to the biaxial strain. Further examination of the behavior of the different states shows that the peaks are shifted by the biaxial strain. The occupied majority-spin Δ_1 state shifts to higher energy, which is attributed to the enhancement of the repulsive force between the interfacial Fe and O atoms induced by the reduced Fe–O bond length. Meanwhile, the majority-spin Δ_1 states at

the Fermi level decrease as the biaxial strain increases. Conversely, the occupied majority-spin Δ_2 ($d_{x^2-y^2}$) state shifts to lower energy because of the reduced repulsive force due to the increased distance between the in-plane Fe atoms under the biaxial strain. Several electrons in the minority-spin antibonding orbital under the $\Delta_{2'}$ Bloch state shift to the bonding orbital. Therefore, the minority-spin $\Delta_{2'}$ orbital will accommodate more electrons. Thus, the spin-polarized Bloch states of the interfacial Fe atoms in the Fe/MgO interface may be unstable under the biaxial strain, and the electrons may transfer from Δ_1 orbital into Δ_2 and $\Delta_{2'}$ orbitals as the biaxial strain increases. Orbital-decomposed DOS of the interfacial Fe and Co atoms in the CoFe/MgO interface are shown in Figs. 4(b) and 4(c), respectively. The minority-spin Δ_1 states of Fe atom at the Fermi level are relatively smaller than those at the Fe/MgO interface, which is expected to be more stable under the biaxial strain. Given that Co atom has an additional 3d electron compared to Fe atom, the interaction between these atoms results in the electron transport from interfacial Co into Fe atom. Further comparison of the four Bloch states between the Fe and Co atoms shows that the $\Delta_{2'}$ and Δ_5 states of the Fe atom have the same bandwidth and spin split energy as those of the Co atom and, in particular, they show the same shift behavior under the biaxial strain. This phenomenon indicates that the electrons transport from the interfacial Co into Fe atom mainly through the $\Delta_{2'}$ and Δ_5 states. This process will suppress the electron transport between the Δ_1 and $\Delta_{2'}$ states for the interfacial Fe atom, effectively stabilizing the Fe Δ_1 state as the biaxial tensile strains increase. However, for the interfacial Co atom, the Δ_1 state shifts to higher energy, indicating the electron transport from the Δ_1 state into the other states. Consequently, the majority-spin Δ_1 state of the Co atom at the center of the 2DBZ is reduced and finally disappears under increasing biaxial strain. The majority-spin Δ_1 states for Fe and Co at Fermi level in CoFe/MgO interfaces decrease as the biaxial strain increases, similar to that in Fe/MgO interface.

Figures 5(a) and 5(b) show the orbital-decomposed DOS of the interfacial Fe and Co atoms in the CoFeB/MgO interface, respectively. Similar to those of the Fe/MgO and CoFe/MgO interfaces, the four majority-spin Bloch states are highly occupied and the minority-spin Bloch states are partially occupied in the unstrained and strained CoFeB/MgO interfaces. The majority-spin Δ_1 states at the Fermi level for Fe and Co in the CoFeB/MgO interfaces increase as the biaxial strain increases, and this trend is contrary to that in the Fe/MgO and CoFe/MgO interfaces. Comparison of the different states in the CoFeB/MgO interface with those in the CoFe/MgO interface shows that all bonding states of the Fe and Co atoms in the CoFeB/MgO interface shift to lower energy. This phenomenon can be attributed to the bonding states produced by the hybridization between B 2p and Fe (Co) 3d orbitals. The downshift of these states leads to the significant diminution of the minority-spin $\Delta_{2'}$ and Δ_5 states at the Fermi level for the interfacial Fe and Co atoms, which is beneficial for electronic stability under the biaxial strain. Moreover, the B-Fe and B-Co (2p-3d) bonding states will suppress the charge redistribution between the $\Delta_{2'}$ and Δ_1 orbitals as the biaxial tensile strain increases. This phenomenon leads to more stable interface states for the CoFeB/MgO interface.

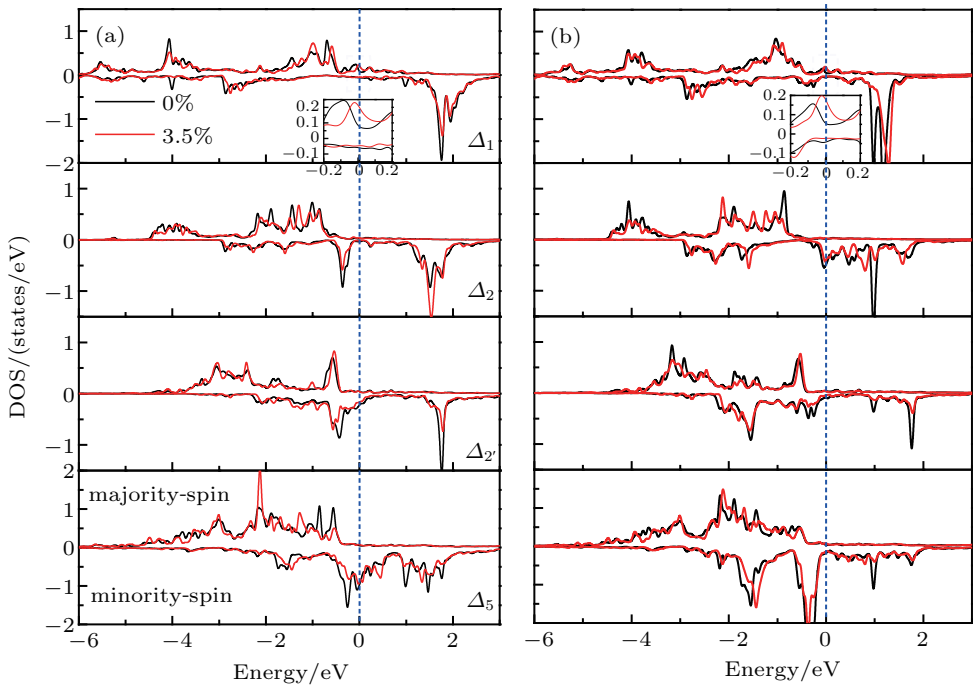


Fig. 5. (color online) Orbital-decomposed DOS in the CoFeB/MgO interfaces for the interfacial (a) Fe and (b) Co atoms. Details around E_F for the Δ_1 state are shown in the inset. The red and black lines correspond to biaxial strains of 0% and 3.5%, respectively.

The majority-spin Δ_1 state coupling between the FM and MgO layers is critical for the TMR ratio of MgO-based MTJs. The relative TMR values of MTJ for the three FM/MgO interfaces with or without biaxial strain are estimated by calculating the layer-projected wave function of the majority-spin Δ_1 Bloch state at the Fermi level (Fig. 6). The decay rates of the majority-spin Δ_1 state in the MgO layers are determined by fitting the wave function in the MgO layers, and the results are summarized in Table 2. The decay rates for the unstrained Fe/MgO, CoFe/MgO, and CoFeB/MgO interfaces are 1.46, 1.44, and 1.42, respectively, which agree well with the previous results.[14] Compared with that of the unstrained interface, the decay rate is strongly enhanced to 2.84 under 3.5% tensile biaxial strain for the Fe/MgO interface, which leads to a significant reduction in the amplitude of the Δ_1 state within MgO. Meanwhile, the decay rates of the Δ_1 state only slightly increase to 1.58 and 1.43 in the 3.5% strained CoFe/MgO and CoFeB/MgO interfaces, respectively. This result suggests that the majority-spin wave function with the Δ_1 symmetry still can efficiently transport in the MgO layers for the CoFe/MgO and CoFeB/MgO interfaces under high biaxial strain. In addition, the majority-spin Δ_1 Bloch state exhibits a smoother evolution tendency in the strained CoFeB/MgO than that of the strained CoFe/MgO interface, indicating a more stable transport property for the CoFeB/MgO interface. Given the large biaxial strain induced by lattice mismatch, the MTJ with CoFeB/MgO interface is expected to maintain a higher TMR value. This phenomenon indicates another origin for the enhanced performance of CoFeB/MgO MTJs.

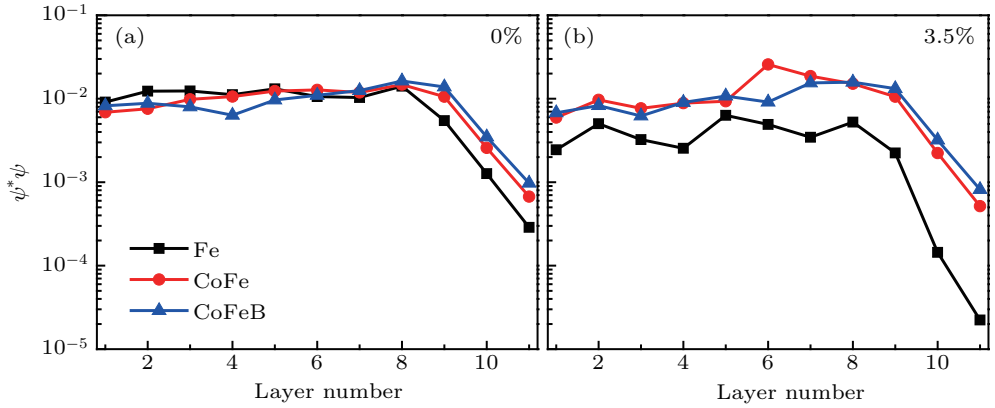


Fig. 6. (color online) Majority-spin Δ_1 Bloch state characters around the Fermi level as a function of layer number for the Fe/MgO, CoFe/MgO, and CoFeB/MgO interfaces (a) without and (b) with 3.5% tensile biaxial strain, respectively.

Table 2. Decay rates of the majority-spin Δ_1 state in MgO layers for the three FM/MgO interfaces without and with 3.5% biaxial tensile strain.

Biaxial tensile strain	0%	3.5%
Fe/MgO	1.46	2.84
CoFe/MgO	1.44	1.58
CoFeB/MgO	1.42	1.43

4. Conclusion

The effects of biaxial tension strain on the electronic structure and the spin-related state coupling in the Fe/MgO, CoFe/MgO, and CoFeB/MgO interfaces are investigated using first-principles calculations. The $k_{||}$-resolved density of majority-spin Δ_1 state for the three interfaces is calculated to determine the strain-dependent coupling efficiency between the FM and MgO layers. As the biaxial strain increases, the state coupling between the Fe and MgO layers is seriously attenuated in the Fe/MgO interface. Moreover, the coupling channel is mostly closed when the biaxial strain exceeds the threshold value of 2.8%. The majority-spin Δ_1 state of Fe atom in the CoFe/MgO interface is more stable and can still be coupled into MgO under large biaxial strain. The interfacial Co atom also opens up a coupling channel, which is closed under a higher threshold strain of 3.5%. The CoFeB/MgO interface, which is superior to the other two tested interfaces, maintains larger coupling channels for the majority-spin Δ_1 state under large biaxial strain. The coupling efficiency through both the interfacial Fe and Co atoms into MgO is obviously enhanced with this interface. Orbital-decomposed DOS for the interfacial Fe and Co atoms are calculated to reveal the internal mechanism of the redistribution of the majority-spin Δ_1 state. Accordingly, the bonding interactions between the Fe, Co, and B atoms and the electron transfer between different Bloch states are deduced, which well explain the strain-dependent coupling efficiency between the FM and MgO layers. In addition, layer-projected wave function of the majority-spin Δ_1 Bloch state is calculated, and the results suggest slower decay rate and more stable transport property for the CoFeB/MgO interface. Therefore, the MTJ with CoFeB/MgO interface is expected to maintain a higher TMR value under large biaxial strain. This work provides some references to the design and manufacturing of MTJs with enhanced TMR effect.

References

[1] Žutić I, Fabian J and Das Sarma S 2004 *Rev. Mod. Phys.* **76** 323
[2] Fert A 2008 *Rev. Mod. Phys.* **80** 1517
[3] Ohno H 2010 *Nat. Mater.* **9** 952
[4] Wolf S A, Awschalom D D, Buhrman R A, Daughton J M, von Molnar S, Roukes M L, Chtchelkanova A Y and Treger D M 2001 *Science* **294** 1488
[5] Syed Sheraz Ahmad W H, Tang J, Zhang Y S, Hu B, Ye J, Gul Q, Zhang X Q and Cheng Z H 2016 *Chin. Phys. B* **25** 97501
[6] Parkin S S P, Roche K P, Samant M G and Rice P M 1999 *J. Appl. Phys.* **85** 5828
[7] Mistral Q, Deac A, Grollier J, Redon O, Liu Y, Li M, Wang P, Dieny B and Devolder T 2006 *Materials Science & Engineering B* **126** 267
[8] Pannetier M, Fermon C, Le G G, Simola J and Kerr E 2004 *Science* **304** 1648
[9] Ripka P and Janosek M 2010 *Sensors Journal IEEE* **10** 1108
[10] Meservey R and Tedrow P M 1994 *Physics Reports* **238** 173
[11] Maekawa S and Inoue J 1996 *J. Magn. Magn. Mater.* **156** 315
[12] Liu Y, Zhu K G, Zhong H C, Zhu Z Y, Yu T and Ma S D 2016 *Chin. Phys. B* **25** 117805
[13] Mathon J and Umerski A 2001 *Phys. Rev. B* **63** 220403
[14] Butler W H, Zhang X G, Schulthess T C and MacLaren J M 2001 *Phys. Rev. B* **63** 054416
[15] Yuasa S and Djayaprawira D D 2007 *J. Phys. D: Appl. Phys.* **40** R337
[16] Yuasa S, Nagahama T, Fukushima A, Suzuki Y and Ando K 2004 *Nat. Mater.* **3** 868
[17] Parkin S S, Kaiser C, Panchula A, Rice P M, Hughes B, Samant M and Yang S H 2004 *Nat. Mater.* **3** 862
[18] Zhang X G and Butler W H 2004 *Phys. Rev. B* **70** 172407
[19] Ikeda S, Hayakawa J, Ashizawa Y, Lee Y M, Miura K, Hasegawa H, Tsunoda M, Matsukura F and Ohno H 2008 *Appl. Phys. Lett.* **93** 082508
[20] Zhang X G, Butler W H and Bandyopadhyay A 2003 *Phys. Rev. B* **68** 092402
[21] Ke Y, Xia K and Guo H 2010 *Phys. Rev. Lett.* **105** 236801
[22] Miao G X, Park Y J, Moodera J S, Seibt M, Eilers G and Münzenberg M 2008 *Phys. Rev. Lett.* **100** 246803
[23] Wang Y, Zhang J, Zhang X G, Cheng H and Han X F 2010 *Phys. Rev. B* **82** 054405
[24] Ma Q L, Iihama S, Kubota T, Zhang X M, Mizukami S, Ando Y and Miyazaki T 2012 *Appl. Phys. Lett.* **101** 122414
[25] Guo F, Wu Z, Chen T, Wu Y, Cai G and Kang J 2015 *Computational Materials Science* **101** 138
[26] He K H and Chen J S 2012 *J. Appl. Phys.* **111** 07c109
[27] Ong P V, Kioussis N, Amiri P K, Wang K L and Carman G P 2015 *J. Appl. Phys.* **117** 17b518
[28] Löhndorf M, Duenas T, Tewes M, Quandt E, Rührig M and Wecker J 2002 *Appl. Phys. Lett.* **81** 313
[29] Bonell F 2010 *Phys. Rev. B* **82** 092405
[30] Burke K, Werschnik J and Gross E K U 2005 *J. Chem. Phys.* **123** 062206
[31] Parr B R and Yang W 1989 *Horizons of Quantum Chemistry* (New York: Oxford University Press) pp. 5–15
[32] Car R and Parrinello M 1985 *Phys. Rev. Lett.* **55** 2471
[33] Kresse G and Furthmüller J 1996 *Phys. Rev. B* **54** 11169
[34] Blöchl P E 1994 *Phys. Rev. B* **50** 17953
[35] Kresse G and Joubert D 1999 *Phys. Rev. B* **59** 1758
[36] Perdew J P, Burke K and Ernzerhof M 1996 *Phys. Rev. Lett.* **77** 3865
[37] Chadi D J 1977 *Phys. Rev. B* **16** 1746
[38] Methfessel M and Paxton A T 1989 *Phys. Rev. B* **40** 3616
[39] Kanaji T, Asano K and Nagata S 1973 *Vacuum* **23** 55
[40] Lawler J F, Schad R, Jordan S and Kempen H V 1997 *J. Magn. Magn. Mater.* **165** 224
[41] Li C and Freeman A J 1991 *Phys. Rev. B* **43** 780
[42] Nguyen M C, Zhao X, Ji M, Wang C Z, Harmon B and Ho K M 2012 *Journal of the Optical Society of America A Optics Image Science & Vision* **29** 695
[43] Olsson P, Klaver T P C and Domain C 2010 *Phys. Rev. B* **81** 054102
[44] Burton J D, Jaswal S S, Tsymbal E Y, Mryasov O N and Heinonen O G 2006 *Appl. Phys. Lett.* **89** 142507
[45] Urano T and Kanaji T 1988 *J. Phys. Soc. Jpn.* **57** 3403
[46] Wortmann D, Bihlmayer G and Blügel S 2004 *J. Phys.: Condens. Matter* **16** S5819
[47] Zhang X G and Butler W H 2003 *J. Phys.: Condens. Matter* **15** R1603